Enhanced energy conversion of up-conversion solar cells by the integration of compound parabolic concentrating optics

Solar Energy Materials & Solar Cells 140 (2015) 217–223

Contents lists available at ScienceDirect

Solar Energy Materials & Solar Cells

journal homepage: www.elsevier.com/locate/solmat

Enhanced energy conversion of up-conversion solar cells by the integration of compound parabolic concentrating optics

Georgios E. Arnaoutakis [a,*], Jose Marques-Hueso [a], Aruna Ivaturi [a], Stefan Fischer [b], Jan C Goldschmidt [b], Karl W. Krämer [c], Bryce S. Richards [d,e,**]

[a] Institute of Photonics & Quantum Sciences, Heriot-Watt University, Edinburgh EH14 4AS, United Kingdom
[b] Fraunhofer Institute for Solar Energy Systems, Heidenhofstrasse 2, 79110 Freiburg, Germany
[c] Department of Chemistry and Biochemistry, University of Bern, Freiestrasse 3, CH-3012 Bern, Switzerland
[d] Institute of Microstructure Technology (IMT), Karlsruhe Institute of Technology, Hermann-von-Helmholtz-Platz 1, 76344 Eggenstein-Leopoldshafen, Germany
[e] Light Technology Institute (LTI), Karlsruhe Institute of Technology, Engesserstrasse 13, Building 30.34, 76131 Karlsruhe, Germany

ARTICLE INFO

Article history:
Received 20 September 2014
Received in revised form
7 April 2015
Accepted 8 April 2015

Keywords:
Photovoltaics
Up-conversion
Erbium
Silicon
Compound parabolic concentrator
Integrated optics

ABSTRACT

Up-conversion (UC) is a promising approach to utilize sub-band-gap photons for solar cells (SCs). Due to the non-linear nature of UC, the optimal excitation power regimes between the solar cell semiconductor and the UC material correspond to a difference in solar concentration of more than an order of magnitude. This difference can be bridged with integrated optics by concentrating the photons transmitted through the solar cell to increase the power density and maximize the intensity of UC luminescence. To realize this, dielectric-filled compound parabolic concentrators (CPCs) were used as integrated optics on the rear side of a planar bifacial silicon solar cell together with a 25% Er^{3+} doped hexagonal sodium yttrium fluoride (β-$NaYF_4$:Er) UC phosphor. An efficiency increase of 32% from 0.123% to 0.163% under sub-band-gap illumination is quantified by means of the first ever reported *I–V* characteristics for an up-conversion solar cell (UC-SC) based on c-Si. An enhancement in external quantum efficiency (EQE) is obtained from 1.33% for the non-concentrating reference UC-SC to 1.80% for a solar cell with integrated optics for an excitation at 1523 nm with an irradiance of 0.024 W/cm^2, corresponding to a normalized EQE of 0.75 W/cm^2. This demonstrates that CPCs are suitable for UC-SC as they increase the concentration in the forwards direction, while maintaining high collection efficiency of the UC emission in the reverse direction. In addition, such an approach enables the optimization of the solar concentration on the UC phosphor independently from the concentration required for the solar cell.

1. Introduction

Among the spectral conversion approaches [1–3] to overcome the Shockley–Queisser efficiency limit for single-junction solar cells (SCs) [4], up-conversion (UC) aims to recover sub-band-gap photons otherwise transmitted through a solar cell. It has been theoretically estimated that UC can provide a relative efficiency increase of approximately 25% on an overlying silicon solar cell with band-gap $E_g = 1.12$ eV [5,6], while under solar concentration of 46,200 Sun the theoretical limit was predicted to be 53% [7]. Given that UC is a non-linear process, high solar concentration would be beneficial for UC in order to maximize the emission of high energy photons from each pair of low energy photons. For an ideal UC process this emission has quadratic relation to power; however due to conservation of energy it will saturate at high powers depending on the dominant mechanism of depopulation [8] leading to a non-linear relation with power. This would also result in saturation of the photoluminescence quantum yield (PLQY) defined as the ratio of emitted photons to either a) absorbed photons for internal PLQY (iPLQY) or b) incident photons for external PLQY (ePLQY).

One of the most efficient UC phosphors, 25% Er^{3+}-doped hexagonal sodium yttrium fluoride (also referred to as β-$NaYF_4$:25% Er^{3+} or β-$NaEr_{0.25}Y_{0.75}F_4$) has recently been reported with ePLQY of $6.6 \pm 0.7\%$ under broadband excitation of 1.97 MW/m^2 [9]. Upon $^4I_{15/2}$ to $^4I_{13/2}$ excitation of Er^{3+} around 1520 nm this phosphor shows a strong $^4I_{11/2}$ to $^4I_{15/2}$ emission around 980 nm due to energy transfer up-conversion (ETU). This phosphor exhibits saturation at a power density above 10^4 W/m^2 which agrees well with extrapolated iPLQY under monochromatic excitation [10]. The equivalent solar

* Corresponding author.
** Corresponding author at: Institute of Microstructure Technology (IMT), Karlsruhe Institute of Technology, Hermann-von-Helmholtz-Platz 1, 76344 Eggenstein-Leopoldshafen, Germany.
E-mail addresses: G.E.Arnaoutakis@gmail.com (G.E. Arnaoutakis), bryce.richards@kit.edu (B.S. Richards).

http://dx.doi.org/10.1016/j.solmat.2015.04.020

concentration can be defined as

$$C_{exc} = \frac{\int_{\lambda_1}^{\lambda_2} P_{exc}(\lambda)\partial\lambda}{\int_{\lambda_1}^{\lambda_2} P_{AM1.5D}(\lambda)\partial\lambda}, \quad (1)$$

where P_{exc} is the excitation power density or irradiance at the respective wavelength, $P_{AM1.5D}$ the spectral irradiance of the air-mass 1.5 direct (AM1.5D) solar spectrum [11] between λ_1 and λ_2, the integration limits corresponding to the absorption band of the UC phosphor. For β-$NaYF_4$:Er with an absorption between 1450 and 1590 nm and the power density of 10^4 W/m^2 as mentioned above, this scales to a solar concentration of more than 350 × the integrated solar irradiance in this range (28 W/m^2). Equivalent or higher solar concentration levels are currently utilized in high concentration photovoltaic systems [12].

A relation similar to the PLQY follows for the external quantum efficiency (EQE) of an up-conversion solar cell (UC-SC) with power, as

$$\mathrm{EQE} \propto \frac{P^n}{P} \propto P^{n-1}, \quad (2)$$

where P is the power density and n the integer number of low energy photons resulting in UC. Although the exponent n follows the theoretical value at low irradiance, from experimental studies [13,14] it has been observed to be considerably lower at high irradiance.

The incident power relates to the concentration of the solar spectrum which can be quite different between the solar cell and the UC phosphor. Therefore, it would be useful to distinguish between C_{exc} and the more widely known concentration factor C_{inc} defined by the incident irradiance on the operating wavelength range of the solar cell P_{inc}, as

$$C_{inc} = \frac{\int_{\lambda_1}^{\lambda_2} P_{inc}(\lambda)\partial\lambda}{\int_{\lambda_1}^{\lambda_2} P_{AM1.5D}(\lambda)\partial\lambda}, \quad (3)$$

To obtain the concentration incident on the solar cell, from Eqs. (1) and (3) it would be

$$C_{inc} = \frac{\int_{\lambda_1}^{\lambda_2} P_{exc}(\lambda)\partial\lambda}{C_{geo}\int_{\lambda_1}^{\lambda_2} P_{AM1.5D}(\lambda)\partial\lambda}, \quad (4)$$

where C_{geo} is the required concentration between the solar cell and the UC phosphor. For silicon solar cells the conversion efficiency is maximized at approximately 100 Sun due to increased series resistance above this solar concentration [15,16]. As a consequence, an UC-SC would require a form of optical management to obtain the required concentration C_{exc}.

A more generic formulation of the problem to be solved can be approached from conservation of entropy. The generalized étendue at the input of the optics should equal the étendue at the output, therefore [17]

$$n_1^2 A_1 \int \cos\theta_1 d\Omega_1 = n_2^2 A_2 \int \cos\theta_2 d\Omega_2, \quad (5)$$

where n is the index of refraction, Ω the solid angle, θ the acceptance angle, and A the aperture of the optics, while indices 1 and 2 refer to input and output, respectively. Additionally, the maximum average solar concentration in three-dimensional space can be estimated by the angular ratio [17]

$$\frac{n_2^2 \sin^2\theta_2}{n_1^2 \sin^2\theta_1}. \quad (6)$$

However, the spatial distribution of the concentration (and hence the power density) at the output of the optics will vary significantly from the average and can be modeled *via* ray optics. For an UC-SC, this power density is of particular interest as it relates with the UC luminescence and the EQE as indicated in Eq. (2).

Current approaches for optical management include coupling of the localized electric fields *via* plasmon resonance [18–23], photonic crystals [24–26], or a combination of both [27] to effectively enhance the local density of optical states in the neighboring Er^{3+} ions. Geometrical concentration can also be utilized with integrated macro-scale optics such as slanted metalized back contacts [28], luminescent concentrators [29], or micro-structured back reflectors [30]. Such integrated optics can potentially bridge the mismatch in concentration between UC phosphor and solar cell.

A comparative study [31] between imaging and non-imaging optics has recently analyzed the limitations of the former and identified the advantages of the latter for integration in UC-SC which are three-fold: i) concentration of transmitted photons through the solar cell to excite the UC phosphor, ii) high transmission of the excitation over a broad range in the near-infrared (NIR), and iii) high collection efficiency of the isotropic emission from the UC phosphor back to the solar cell. It is highlighted that the collection of the isotropic emission shares common traits with the restriction in the angle of emission. This has been conceptualized as another approach to overcome the limiting efficiency of solar cells [32,33] by taking advantage of the external radiative emission of a solar cell [34,35].

In this paper we focus on the properties of the best performing non-imaging optics as mentioned above and particularly in dielectric-filled compound parabolic concentrators (CPCs). An artistic impression of the concept utilizing CPC in UC-SC is depicted in Fig. 1(a). We proceed by investigating the questions of how the angle of acceptance of the CPC – and therefore the angle for the collection of the emitted luminescence – can enhance the EQE of an UC-SC in Section 3.2 and how the EQE is affected by the incident power in Section 3.3. Finally, the performance of an UC-SC is quantified *via* current-voltage (*I–V*) characteristics presented in Section 3.4, the first ever reported for UC-SC based on c-Si to the best of the authors' knowledge.

2. Materials and methods

A three-dimensional model based on ray optics and Monte Carlo simulations (Optis, Optisworks) was used for spatially resolved considerations, where the entry aperture of the CPC was illuminated with the maximum power available in the experimental configuration transmitted through the solar cell. This corresponds to a power density of 0.019 W/cm^2 and solar concentration C_{inc} of 6.8 Sun. The UC phosphor coupled at the exit aperture of the CPC was also modeled with optical properties taken from reference [36]. A schematic of the UC-SC and the optical setup used for characterization is shown in Fig. 1(b). Illumination between 1450 and 1590 nm from a NIR tunable laser (HP-Agilent, 8168 -F, 6 mW at 1523 nm) was used, fiber-coupled, and collimated. This resulted in a beam of second moment width of ($d4\sigma$) 4.2 mm and divergence of 0.02°, spatially characterized by a NIR camera (Electrophysics, Micronviewer 7290A), and the power measured with a calibrated germanium photodiode (Newport, 818-IR). A source-meter (Keithley Instruments, 2440-C) was used to measure the *I–V* characteristics of the UC-SC, as well as the photo-generated short circuit current (I_{sc}) to determine the EQE. No additional optical bias was used and the setup was enclosed to prevent any interference with the room lighting.

The UC-SC were based on planar bifacial solar cells fabricated on silicon wafers (1 Ω cm, 200 μm-thick, *n*-type float zone) with aluminum oxide (Al_2O_3) surface passivation on both front and rear surfaces. The solar cells feature anti-reflection coatings (ARC) optimized for high transmittance of sub-band-gap photons, with a double layer ARC (110 nm hydrogenated silicon nitride (a-SiN_x:H)

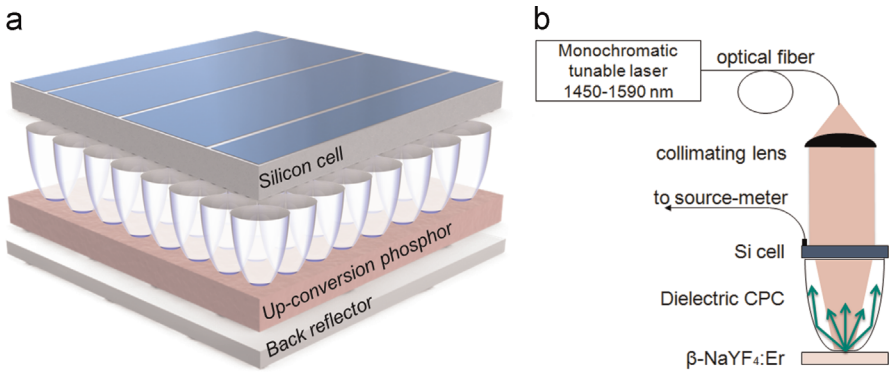

Fig. 1. (a) Artistic impression of the UC-SC with a regular two-dimensional array of integrated CPC optics. The gaps between the layers are only for illustrative reasons. (b) Schematic and optical setup used for characterization. The three-fold role of the optics – concentration, broadband transmission of the excitation (light red beam) and coupling of the isotropic emission (green arrows) – is depicted (For interpretation of the references to color in this figure legend, the reader is referred to the web version of this article).

and 110 nm magnesium fluoride (MgF_2)) on the front and a single layer ARC (120 nm a-SiN_x:H) on the rear. This yielded a solar cell that exhibited an excellent EQE for rear-side illumination with 980 nm. A detailed description of the solar cells, their performance and optimization is beyond the scope of this paper and can be found elsewhere [37].

Two geometries of CPC (Edmund Optics) were used with acceptance angles of 25° and 45°, denoted as CPC-25° and CPC-45° henceforth, with entry apertures of 9.01 mm and 5.39 mm, lengths of 19.93 mm and 7.52 mm, respectively, and an exit aperture of 2.5 mm for both. The dielectric used for both CPC was B270 borosilicate glass, without ARC deposited on any of the apertures other than a refractive index matching liquid (Cargille, L-RIA-766, $n=1.53$ at 589.2 nm) for optical coupling between the elements.

The UC material consisted of β-$NaYF_4$ micro-phosphors doped with 25% Er^{3+} cast in a perfluorocyclobutane (PFCB) polymer (Tetramer Technologies LLC, USA) matrix. The phosphor-to-polymer weight ratio was 84.9% and the material was prepared according to the methods in references [38,39].

Although it has already been suggested that the CPC may be combined with a lens of positive focal length as a primary optic on the solar cell [17,31], this aspect is part of further system integration [40,41] and will not be considered in this paper. Therefore, all experiments in this paper are performed with the illumination at normal incidence despite the wider acceptance angle of the optics.

3. Results and discussion

3.1. Spatial distribution of power

The irradiance profile at the exit aperture of the two CPC geometries is displayed in Fig. 2, as obtained by Monte Carlo simulations. The average power density at the input and output is 0.019 W/cm^2 and 0.053 W/cm^2, respectively, for both CPC. This corresponds to a geometrical concentration C_{geo} of 2.79× and an optical transmission above 98%.

It can be seen that for both CPC the profile is uniform around the center of the exit aperture, as expected for rays transmitted without reflection on the side of the parabola. Localized peaks that maximize towards the edges of the exit aperture are also observed due to the characteristic concentration profile of the parabolas. For the CPC-45° the local maxima of 0.21 W/cm^2 are at ±0.80 mm from the center, while for the CPC-25° the maxima of 0.41 W/cm^2 are observed at ±0.32 mm.

The CPC-25° exhibits higher maxima than the CPC-45° as a result of the curvature of the 45° parabola reflecting more rays towards the

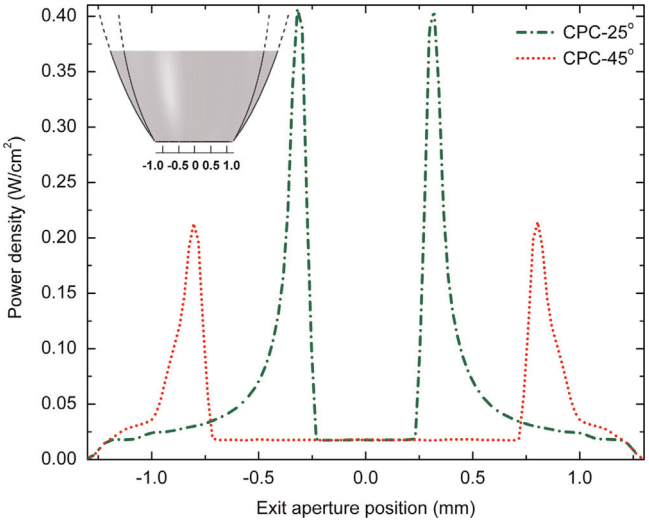

Fig. 2. Distribution of the power density at the exit aperture of each CPC under normal incidence. The CPC are illuminated with light of 1523 nm and at the maximum power available in the experiment after transmission through the solar cell (0.019 W/m^2 or 7 suns).

edges of the aperture. To explain this aspect it is informative to mention that the CPC is designed according to the edge-ray principle. Subsequently, all the incident rays at the maximum (designed) acceptance angle are being reflected at the parabola and focused at the edge of the exit aperture. For a given design, as the condition for acceptance is relaxed and the angle is approaching normal incidence, the distribution of rays is deviating from the edge towards the center of the exit aperture. In other words, the parabola of the CPC-45° is more abrupt in relation to the exit aperture than the CPC-25° (see inset in Fig. 2). Therefore, for rays perpendicularly incident on the parabola of the CPC-25°, the angle of reflection would be higher, consequently concentrating more rays towards the center of the exit aperture compared to the CPC-45°.

Following this notion, the acceptance angle can be further reduced to result in even higher local concentration. Additionally, the exit aperture is further reduced, while keeping the entry aperture constant to allow for comparison with experimental data in this configuration. It is noted that smaller angles and exit apertures will result in longer optics that can be further optimized *via* truncation, however to illustrate the purposes of the current design these will not be considered here. Fig. 3 shows the irradiance profile at the exit apertures of two CPC with acceptance angles of 4° and 2°, and exit apertures of 200 μm and 100 μm, respectively (CPC-4° and CPC-2°). The irradiance profile of the CPC-2°and CPC-4° resembles the profile

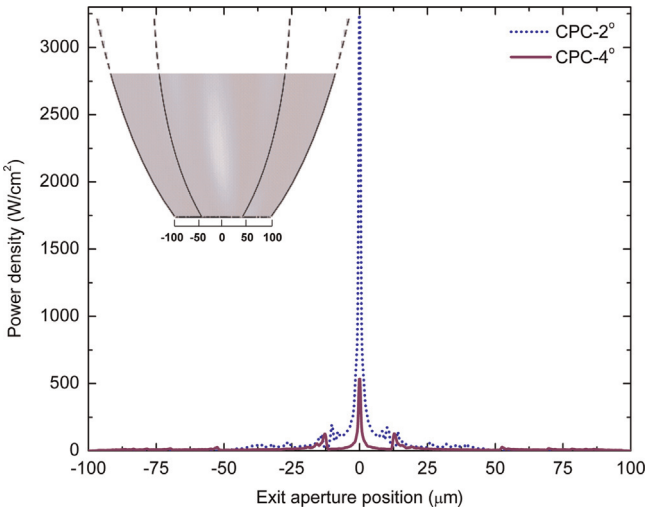

Fig. 3. Distribution of the power density at the exit aperture of CPC-4° and CPC-2° with apertures 200 μm and 100 μm, respectively. The illumination and modeling conditions are identical to these of Fig. 2 to allow for direct comparisons.

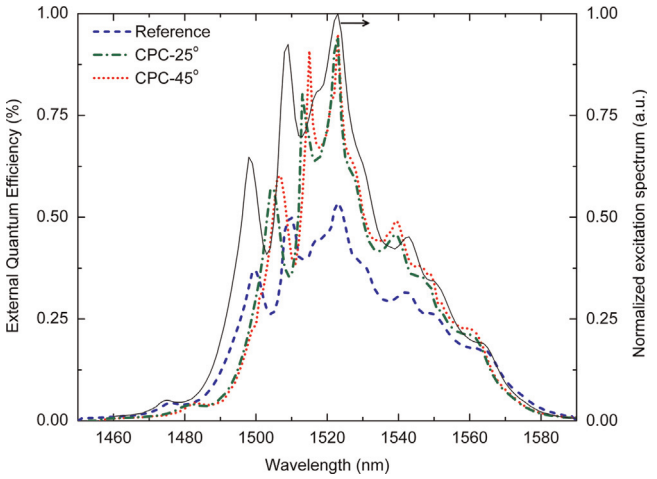

Fig. 4. EQE of the UC-SC without (reference) and with two different CPC geometries characterized at 0.01 W/cm^2. The shift of the peaks between the UC-SC is an artifact of the software used for acquisition of the spectra. The excitation spectrum of the $^4I_{11/2}$ to $^4I_{15/2}$ UC emission for $^4I_{15/2}$ to $^4I_{13/2}$ excitation of β-$NaYF_4$:Er is also plotted for comparison.

of tapered optics [31, Fig. 8]. However, the backwards transmission of the tapered, important for the EQE of the UC-SC in Section 3.3, is significantly lower than the CPC optics.

The localized peaks are observed at the center of the exit aperture for both CPC as expected. Output peak power densities of 530 W/cm^2 and 3240 W/cm^2 are obtained while the average power densities are 11.92 W/cm^2 and 41.95 W/cm^2 from the CPC-4° and CPC-2°, respectively. From Eq. (1) this would result in solar concentration C_{exc} of 4250 Sun for the CPC-4° and 14,980 Sun for the CPC-2°. Although, this solar concentration is more than 200 × higher compared to the average power density of the CPC-25° and CPC-45°, additional factors will affect the performance of the UC-SC. This aspect is analyzed in the following sections along with the expected enhancement in EQE.

The resultant spatial distribution with the assigned localized peaks will excite the UC phosphor non-uniformly, subsequently altering the rate of transitions between energy levels and more importantly the energy transfer between Er^{3+} ions. However, it has been analytically and numerically confirmed [42] that even for non-linear processes such as UC, a good approximation can be derived for a Gaussian beam with a uniform beam of cylindrical radius and equal beam waist. The latter was also validated in respect to the incident pump power with insignificant effect on the UC emission [8]. This can be determined *via* power dependent characterization of the UC-SC and is discussed further in Section 3.3.

3.2. External quantum efficiency

Fig. 4 shows the EQE of the UC-SC without any optics and with concentrating optics of two different geometries as a function of wavelength between 1450 and 1590 nm and power density of 0.01 W/cm^2.

The highest EQE is obtained at the peak wavelength of the $^4I_{15/2}$ to $^4I_{13/2}$ excitation of β-$NaYF_4$:Er at 1523 nm. For all measured solar cells the EQE agrees with the $^4I_{11/2}$ to $^4I_{15/2}$ UC emission spectrum of β-$NaYF_4$:Er also plotted in Fig. 4 for comparison. This can be one of the indications that the dominant mechanism for depopulation of $^4I_{13/2}$ is ETU between Er^{3+} ions. For the main peak at 1523 nm the CPC devices exhibit similar EQE, while for the weaker peaks the solar cell with CPC-45° has higher EQE than the CPC-25°. Comparing with the EQE of the UC-SC with parabolic optics and 42% transmission c-Si solar cells, *cf.* [31, Fig. 3], this represents a nearly 40 times higher EQE. The improvement is obtained by the higher transmission of the c-Si solar cell, but also the excellent transmission and collection of the CPC optics.

Spectral narrowing of the weaker peaks is observed for the UC-SC with CPC. This suggests that the concentrating effect of the optics effectively alters the macroscopic excitation profile (shown in Fig. 2) and affects the probability of ETU on the microscopic level. Shifting is observed for the UC-SC with CPC-45° (3–8 nm) and smaller for the UC-SC with CPC-25° (1–6 nm) which is an experimental artifact of the software used for acquisition of the spectra. The spectral shape of the UC excitation spectrum varies with increasing excitation power since excited state populations increase and also higher lying Stark levels are populated due to a rising sample temperature [43]. Accordingly, UC emissions from the higher lying $^4F_{9/2}$, $^4S_{3/2}$, and $^2H_{11/2}$ states, populated by more than two photon processes [44], contribute to the photocurrent of the silicon solar cell. Intense green luminescence due to the $^2H_{11/2}$ and $^4S_{3/2}$–$^4I_{15/2}$ transitions was observed by naked eye under the conditions of the characterization reported here, which corroborates the latter hypothesis.

Although the EQE of the UC-SC in Fig. 4 was obtained at a constant incident power density of 0.01 W/cm^2, the power density exciting the UC phosphor varies locally according to the concentration achieved by the CPC optics, see Fig. 2. As discussed in the previous section, despite that the average power density is equal for both CPC, the maximum local power density for the UC-SC with the CPC-25° is significantly higher than this of the CPC-45°. Consequently, a higher EQE was expected for the UC-SC with CPC-25°. For increasing power density however, saturation of the EQE is also expected [13,14], which is evidenced by the observed response at the above mentioned power density. Nevertheless, due to the non-linear nature of UC and hence UC-SC, a power dependent characterization is required to investigate for lower and higher pump regimes. This follows in the next section.

3.3. Power dependence

The EQE as a function of incident power is displayed in Fig. 5 as open symbols for the reference and the UC-SC with integrated CPC. In the low power regime (0.0047–0.028 W/cm^2) the EQE is enhanced for both CPC devices by a factor of 2.7 × from 0.13% to 0.37% and 0.35% for the reference UC-SC compared to the CPC-25° and CPC-45°, respectively. The enhancement is lower for the high power regime (0.028–0.057 W/cm^2) from 1.33% to 1.58% and 1.80%,

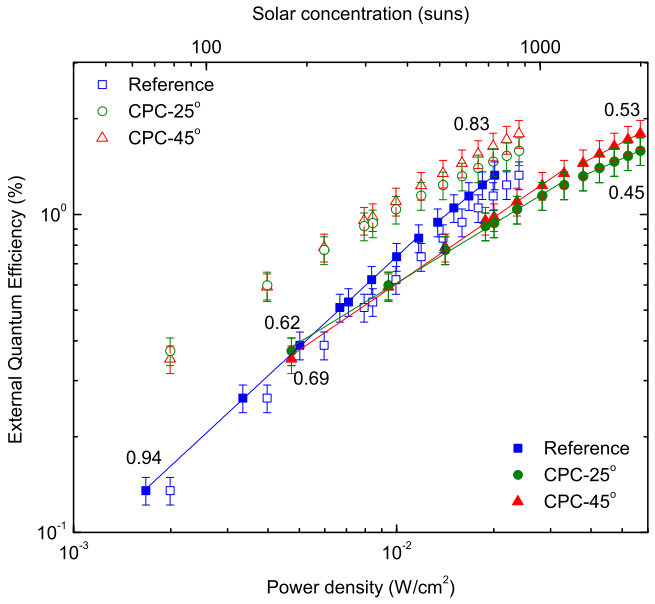

Fig. 5. EQE of the UC-SC for the strongest excitation peak at 1523 nm as a function of incident power and monochromatic solar concentration on logarithmic scales. Open symbols correspond to values of power incident on the UC-SC, while solid symbols to power incident on the UC. Enhancements of 2.7 × are observed in the low power regime and 1.3 × in the high power regime of the UC-SC. The slopes of the curves for the various power regimes are given for the three experimental configurations.

respectively. Due to the additional power density on the UC material from the concentration of the integrated optics, the EQE saturates faster at high pump power for the UC-SC with CPC. A stronger pump power populates higher energy levels of erbium and increases the probability of processes competing with ETU [8].

To further analyze this effect, the power density incident on the UC-SC needs to be normalized to the power concentrated by the optics, consequently exciting the UC. This is displayed in Fig. 5 as solid symbols. The maximum equivalent solar concentrations from Eq. (1) are 740 Sun and 2090 Sun for the reference and the CPC devices, respectively. These C_{exc} are high because the monochromatic irradiance $P_{AM1.5D}$ was used at 1523 nm. After normalization of the power density the high power regime of the reference overlaps with the low power regime of the UC-SC with integrated optics. A lower EQE is observed at the low-pump regime of the CPC devices that at this excitation power overlaps with the high-pump regime of the reference.

According to Eq. (2) for a purely two-photon process an exponent equal to 1 is expected. But the slope for the reference starts from 0.94 in the low power regime and decreases to 0.83 in the high power regime, while even lower slopes are observed for the CPC devices. In particular, in the low power regime the slopes are 0.62 and 0.69 for CPC-25° and CPC-45° and change to 0.45 and 0.53 in the high power regime, respectively. The reduced slopes relate to the change in population at the high-pump regime, involving higher order processes and cross relaxation, which compete with ETU and excited state absorption.

For the same incident power on the UC-SC, the power exciting the UC material depends on the concentration achieved by the CPC. Since the beam size and exit aperture for both CPC are equal, the geometrical concentration factor is 2.79 × ; a value that agrees well with the observed enhancement of the EQE in the low power regime. However, the CPC-25° locally concentrates the excitation beam up to 0.41 W/cm^2 which is twice the value obtained for the CPC-45°, see Fig. 2. This can explain the lower slope of CPC-25° in the high power regime of Fig. 5.

It is useful to identify where losses occur in the UC-SC. Approximately 80% of the incident NIR light is transmitted through the c-Si solar cell, while the transmission of the CPC is 98%. The ePLQY of the β-NaYF$_4$:25%Er^{3+} is 1.2% at 0.024 W/cm^2 [39]. The backwards transmission of the CPC-25° and CPC-45° is 98% and 95%, respectively. This is a significant improvement from the previously best performing parabolic optics presented in reference [31, Fig. 5], with a backwards transmission higher than 88% for emission centers above 1 μm. The emission at 980 nm is finally converted to photocurrent in the c-Si solar cell with an EQE of 76.8% [37], indicating additional space for improvements.

An equation of the form EQE$=a+b\,P^n$, where a and b are fitting parameters, was used to fit the experimentally obtained EQE of the CPC-25° UC-SC which exhibits the highest saturation. Furthermore, the expected EQE by extrapolating to power densities of 11.92 W/cm^2 (4250 suns) and 41.95 W/cm^2 (14,980 suns) for the CPC-4° and CPC-2° presented in Section 3.1 could be estimated. An EQE of 5.4% and 8.9% is obtained, respectively. This shows not only that concentration levels C_{exc} of 10^4 Sun are required, corresponding to C_{inc} of 6.78 Sun from Eq. (4), but also that substantial improvements can be achieved by the blending of concentrating systems with UC-SC.

Of course, the design space for more suitable optics is unlimited and several non-imaging optics methods such as the flow line or the simultaneous multiple surface, would be useful to this end. The requirement for higher solar concentrations can be tolerated by optics used on top of the solar cell [45,46] in conjunction with the optics investigated herein. Moreover, the account of optical losses indicates that the EQE of the UC-SC primarily relies on the PLQY of the up-converter. Although β-NaYF$_4$:25%Er^{3+} is among the most efficient up-converters for photovoltaics, the PLQY is constantly improving with the intensive research in new and efficient up-converters [47,48].

The normalized EQE (NEQE) is usually calculated for comparison with UC-SC in the literature. It has to be mentioned, however, that the NEQE is not totally independent from the excitation power density. For the highest incident power of 0.024 W/cm^2 the NEQE were 0.55 cm^2/W for the reference UC-SC, 0.75 cm^2/W for CPC-45°, and 0.66 cm^2/W for the CPC-25° device. These values are in the range of the normalized ePLQY of the UC material for which a value of 0.67 cm^2/W was determined from photoluminescence measurements [39], albeit three times higher than the NEQE values from the recent work by Fischer *et al.* [45], the highest reported NEQE so far to the best of the authors' knowledge. The latter NEQE was obtained for an UC-SC utilizing the same UC phosphor but a lower phosphor to polymer ratio (75.7 w/w%) and an excitation at 1508 nm with 0.1 W/cm^2. Thus the values cannot be compared directly with our results. Nevertheless, it underlines the substantial improvements that can be obtained by concentration and photonic management.

3.4. Current–voltage characteristic

For a more comprehensive characterization of the performance of a solar cell, the *I–V* characteristic is required to indicate equilibrium conditions between photons and carriers as well as the origin of losses in the device [49]. This was measured for the aforementioned UC-SC and is displayed in Fig. 6 with the performance parameters short-circuit current (I_{sc}), open-circuit voltage (V_{oc}), fill factor (FF), and efficiency (η) summarized in Table 1. For all the presented UC-SC, the *I–V* characteristics were measured under dark conditions, and only 1523 nm illumination at incident irradiance of 0.024 W/cm^2 was used.

The current from the un-doped reference solar cell with an undoped β-NaYF$_4$ sample is shown to be negligible. Under sub-band-gap illumination, the I_{sc} is mainly affected by dark current. The additional I_{sc} resulting from UC photons is 0.054 mA for

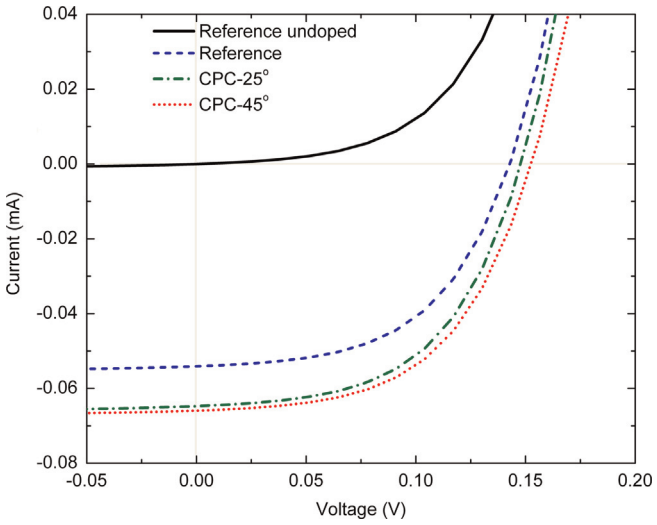

Fig. 6. Current–voltage characteristics of the UC-SC under illumination of 1523 nm at 0.024 W/cm^2. The additional I_{sc} for the UC-SC with concentrating optics is displayed over the reference, while the negligible I_{sc} from the undoped reference solar cell is also displayed.

Table 1
Performance parameters of the UC-SC corresponding to the *I–V* curves in Fig. 6 characterized in the dark, under illumination of 1523 nm at an irradiance of 0.024 W/cm^2.

UC-SC	I_{sc} (mA)	V_{oc} (V)	FF (%)	η (%)
Reference	0.054	0.136	55.38	0.123
CPC-25°	0.065	0.145	54.35	0.154
CPC-45°	0.066	0.153	53.21	0.163

the reference UC-SC, and 0.065 mA and 0.066 mA for the UC-SC with CPC-25° and CPC-45° optics, respectively. The difference between I_{sc} and dark current confirms the origin of the increased I_{sc} from UC in Er^{3+}.

V_{oc} are 0.136 V, 0.145 V, and 0.153 V for the reference, CPC-25°, and CPC-45° UC-SC, respectively. Albeit quite lower than the expected V_{oc} of a good silicon solar cell under AM1.5 G illumination (approx. 0.7 V), these values of V_{oc} result from the low I_{sc} of the UC emission. The reference, CPC-25°, and CPC-45° UC-SC exhibit FF of 55.38%, 54.35%, and 53.21%, respectively. Since the same silicon cell is used for all UC-SC configurations, losses due to series and shunt resistance between silicon and contacts as well as the p–n junction [50] are not expected to contribute to the reduced FF. Moreover, the FF of the silicon cell was independently measured under AM1.5G conditions and was determined as high as 80% [37]. The low FF of the UC-SC presented here are thus attributed to the low illumination conditions. Accordingly, under the conditions of the intended solar application, the solar cell would perform at a V_{oc} as high as 0.7 V. An increased V_{oc} can be expected therefore from the UC-SC, given the contribution of the I_{sc} from the UC additionally to the I_{sc} from photons above the band-gap.

The efficiency, also displayed in Table 1, is extracted from the *I–V* characteristics and translates to 0.123% for the reference while for the CPC-45° and CPC-25° it is 0.163% and 0.154%, respectively. It has to be mentioned however that the presented efficiencies should be considered in relation to the absolute efficiency of the overlying silicon solar cell. Since this efficiency under one sun AM1.5 G conditions is 17.6% [45], the presented UC-SC efficiencies display clearly the contribution of the UC alone and after the enhancement of the concentrating optics. The efficiency improvement achieved by the concentrating optics is marginal compared to the improvement in EQE. This again indicates that the UC-SC is operating at low illumination conditions, *i.e.* the emission from the UC phosphor. At these conditions the additional I_{sc} from the concentrating optics affects only marginally the FF, the V_{oc} and therefore the efficiency. This performance aspect is made apparent by characterizing the UC-SC under open circuit conditions. In fact, characterization so far has been mainly limited to short-circuit conditions, consequently limiting a complete evaluation of the performance of UC-SC. Although another step towards a comprehensive characterization of UC-SC was presented here, additional steps can be foreseen. The effect of sub-band-gap photons along with the photons above the band-gap should be considered in these steps, to exhibit the higher V_{oc}, FF and η. Such steps may comprise of characterization under the standard AM1.5G conditions where solar cells are commonly characterized, and finally under the ambient solar spectrum.

Nonetheless, these results are quite encouraging for UC-SC and highlight that considerable improvement can be gained *via* concentration and photonic management. Further improvements are expected by optimization of the collected properties of the CPC and merit further investigation to indicate the limits of the current design. In addition, advances in two-photon lithography enable three-dimensional fabrication of CPC structures in the micro-scale [51] opening routes for thin-film UC-SC [52].

4. Conclusions

It can be concluded that integration of CPC optics in UC-SC can significantly enhance the EQE. An increase is reported from 1.33% to 1.80% under an excitation of 1523 nm at an irradiance of 0.024 W/cm^2. This improvement is achieved by the concentration of the excitation on the UC phosphor and also efficient collection of the UC emission. Due to the non-linear relation of UC with power, the concentration has an optimum regime where UC luminescence is maximized and competing processes are minimized. This has been exhibited for the UC-SC without and with concentrating optics presented in this paper. Saturation of the EQE is displayed in power dependent measurements and underlines the requirements for photonic management in UC-SC. Increased I_{sc} and V_{oc} of the CPC enhanced UC-SC were also obtained from *I–V* characteristics. The effect of concentration after the solar cell in addition to the effect of the UC phosphor in UC-SC was specified *via* this characterization. This also indicates the performance parameters and the affecting factors that should be considered for further improvements. Additionally to the quantification of the EQE and I_{sc} being widely used in characterization of UC-SC, V_{oc}, FF and finally η provides a comprehensive performance rating. It can finally be suggested, that these performance characteristics should accompany future schemes, to identify routes for improvements and make UC-SC as competitive as other emerging solar cell technologies.

Acknowledgments

The authors would like to thank A. Boccolini, J.A.S Morton, and S. K.W. MacDougall from Heriot-Watt University for valuable discussions. The Engineering and Physical Sciences Research Council (EPSRC) and the European Community's Seventh Framework Program (FP7/2007–2013) supported financially this research *via* Agreement nos. EP/l013245/1 and 246200, respectively.

References

[1] C. Strümpel, M. McCann, G. Beaucarne, V. Arkhipov, A. Slaoui, V. Švrček, C. Del Cañizo, I. Tobias, Modifying the solar spectrum to enhance silicon solar cell

efficiency—an overview of available materials, Sol. Energy Mater. Sol. Cells 91 (2007) 238–249.
[2] E. Klampaftis, D. Ross, K.R. McIntosh, B.S. Richards, Enhancing the performance of solar cells *via* luminescent down-shifting of the incident spectrum: a review, Sol. Energy Mater. Sol. Cells 93 (2009) 1182–1194.
[3] X. Huang, S. Han, W. Huang, X. Liu, Enhancing solar cell efficiency: the search for luminescent materials as spectral converters, Chem. Soc. Rev. 42 (2013) 173–201.
[4] W. Shockley, H.J. Queisser, Detailed balance limit of efficiency of p-n junction solar cells, J. Appl. Phys. 32 (1961) 510–519.
[5] A.C. Atre, J.A. Dionne, Realistic upconverter-enhanced solar cells with non-ideal absorption and recombination efficiencies, J. Appl. Phys. 110 (2011) 034505.
[6] C.M. Johnson, G.J. Conibeer, Limiting efficiency of generalized realistic c-Si solar cells coupled to ideal up-converters, J. Appl. Phys. 112 (2012) 103108.
[7] T. Trupke, M. Green, P. Würfel, Improving solar cell efficiencies by up-conversion of sub-band-gap light, J. Appl. Phys. 92 (2002) 4117–4122.
[8] M. Pollnau, D. Gamelin, S. Lüthi, H. Güdel, M. Hehlen, Power dependence of upconversion luminescence in lanthanide and transition-metal-ion systems, Phys. Rev. B 61 (2000) 3337.
[9] S.K.W. MacDougall, A. Ivaturi, J. Marques-Hueso, K.W. Krämer, B.S. Richards, Broadband photoluminescent quantum yield optimisation of Er^{3+}-doped β-$NaYF_4$ for upconversion in silicon solar cells, Sol. Energy Mater. Sol. Cells 128 (2014) 18–26.
[10] A. Boccolini, J. Marques-Hueso, B.S. Richards, Self-absorption in upconverter luminescent layers: impact on quantum yield measurements and on designing optimized photovoltaic devices, Opt. Lett. 39 (2014) 2904–2907.
[11] C. Gueymard, D. Myers, K. Emery, Proposed reference irradiance spectra for solar energy systems testing, Sol. Energy 73 (2002) 443–467.
[12] R.M. Swanson, The promise of concentrators, Prog. Photovolt.: Res. Appl. 8 (2000) 93–111.
[13] A. Shalav, B.S. Richards, T. Trupke, K.W. Krämer, H.U. Güdel, Application of $NaYF_4$:Er^{3+} up-converting phosphors for enhanced near-infrared silicon solar cell response, Appl. Phys. Lett. 86 (2005) 013505.
[14] S. Fischer, J.C. Goldschmidt, P. Löper, G.H. Bauer, R. Brüggemann, K.W. Krämer, D. Biner, M. Hermle, S.W. Glunz, Enhancement of silicon solar cell efficiency by upconversion: optical and electrical characterization, J. Appl. Phys. 108 (2010) 044912.
[15] R. Sinton, Y. Kwark, J. Gan, R.M. Swanson, 27.5-percent silicon concentrator solar cells, IEEE Electron Device Lett. 7 (1986) 567–569.
[16] A. Mohr, T. Roth, S.W. Glunz, BICON: high concentration PV using one axis tracking and silicon concentrator cells, Prog. Photovolt.: Res. Appl. 14 (2006) 663–674.
[17] R. Winston, J.C. Miñano, P.G. Benitez, Nonimaging Optics, Academic Press, Amsterdam/Boston, MA, 2005.
[18] H. Mertens, A. Polman, Plasmon-enhanced erbium luminescence, Appl. Phys. Lett. 89 (2006) 211107.
[19] T. Aisaka, M. Fujii, S. Hayashi, Enhancement of upconversion luminescence of Er doped Al_2O_3 films by Ag island films, Appl. Phys. Lett. 92 (2008) 132105.
[20] E. Verhagen, L. Kuipers, A. Polman, Field enhancement in metallic sub-wavelength aperture arrays probed by erbium upconversion luminescence, Opt. Express 17 (2009) 14586–14598.
[21] S. Fischer, F. Hallermann, T. Eichelkraut, G. von Plessen, K.W. Krämer, D. Biner, H. Steinkemper, M. Hermle, J.C. Goldschmidt, Plasmon enhanced upconversion luminescence near gold nanoparticles – simulation and analysis of the interactions, Opt. Express 20 (2012) 271–282.
[22] S. Fischer, F. Hallermann, T. Eichelkraut, G. von Plessen, K.W. Krämer, D. Biner, H. Steinkemper, M. Hermle, J.C. Goldschmidt, Plasmon enhanced upconversion luminescence near gold nanoparticles – simulation and analysis of the interactions: errata, Opt. Express 21 (2013) 10606–10611.
[23] A.C. Atre, A. García-Etxarri, H. Alaeian, J.A. Dionne, Toward high-efficiency solar upconversion with plasmonic nanostructures, J. Opt. 14 (2012) 024008.
[24] C. Johnson, P. Reece, G. Conibeer, Theoretical and experimental evaluation of silicon photonic structures for enhanced erbium up-conversion luminescence, Sol. Energy Mater. Sol. Cells 112 (2013) 168–181.
[25] B. Herter, S. Wolf, S. Fischer, J. Gutmann, B. Bläsi, J.C. Goldschmidt, Increased upconversion quantum yield in photonic structures due to local field enhancement and modification of the local density of states—a simulation-based analysis, Opt. Express 21 (2013) A883–A900.
[26] J. Morton, J. Marques-Hueso, B.S. Richards, Enhanced up-conversion for photovoltaics using 2D photonic crystals, in: OSA Renewable Energy and the Environment Congress-Optical Instrumentation for Energy and Environmental Applications, Optical Society of America, Tucson, Arizona United States, 2013, pp. JM3A. 19.
[27] K.Q. Le, S. John, Synergistic plasmonic and photonic crystal light-trapping: architectures for optical up-conversion in thin-film solar cells, Opt. Express 22 (2014) A1–A12.
[28] C. Strümpel, Application of Erbium-doped Up-converters to Silicon Solar Cells, Universität Konstanz, Konstanz, Germany (2007) 119–122.
[29] J.C. Goldschmidt, P. Loper, S. Fischer, S. Janz, M. Peters, S.W. Glunz, G. Willeke, E. Lifshitz, K.W. Krämer, D. Biner, Advanced upconverter systems with spectral and geometric concentration for high upconversion efficiencies, in: IEEE Conference on Optoelectronic and Microelectronic Materials and Devices, IEEE, Sydney, SA, 2008, pp. 307–311.
[30] T.F. Schulze, Y.Y. Cheng, T. Khoury, M.J. Crossley, B. Stannowski, K. Lips, T.W. Schmidt, Micro-optical design of photochemical upconverters for thin-film solar cells, J. Photonics Energy 3 (2013) 034598.
[31] G.E. Arnaoutakis, J. Marques-Hueso, A. Ivaturi, K.W. Krämer, S. Fischer, J.C. Goldschmidt, B.S. Richards, Enhanced up-conversion for photovoltaics *via* concentrating integrated optics, Opt. Express 22 (2014) A452–A464.
[32] M. Peters, J.C. Goldschmidt, B. Bläsi, Angular confinement and concentration in photovoltaic converters, Sol. Energy Mater. Sol. Cells 94 (2010) 1393–1398.
[33] E.D. Kosten, J.H. Atwater, J. Parsons, A. Polman, H.A. Atwater, Highly efficient GaAs solar cells by limiting light emission angle, Light: Sci. Appl. 2 (2013) e45.
[34] M.A. Green, Radiative efficiency of state-of-the-art photovoltaic cells, Prog. Photovolt.: Res. Appl. 20 (2012) 472–476.
[35] O.D. Miller, E. Yablonovitch, S.R. Kurtz, Strong internal and external luminescence as solar cells approach the Shockley–Queisser limit, IEEE J. Photovolt. 2 (2012) 303–311.
[36] J. Gordon, J. Ballato, D.W. Smith, J. Jin, Optical properties of perfluorocyclobutyl polymers. III. Spectroscopic characterization of rare-earth-doped perfluorocyclobutyl polymers, J. Opt. Soc. Am. B 22 (2005) 1654–1659.
[37] M. Rüdiger, S. Fischer, J. Frank, A. Ivaturi, B.S. Richards, K.W. Krämer, M. Hermle, J.C. Goldschmidt, Bifacial n-type silicon solar cells for upconversion applications, Sol. Energy Mater. Sol. Cells 128 (2014) 57–68.
[38] K.W. Krämer, D. Biner, G. Frei, H.U. Güdel, M.P. Hehlen, S.R. Luthi, Hexagonal sodium yttrium fluoride based green and blue emitting upconversion phosphors, Chem. Mater. 16 (2004) 1244–1251.
[39] A. Ivaturi, S.K.W. MacDougall, R. Martín-Rodríguez, M. Quintanilla, J. Marques-Hueso, K.W. Krämer, A. Meijerink, B.S. Richards, Optimizing infrared to near infrared upconversion quantum yield of β-$NaYF_4$:Er^{3+} in fluoropolymer matrix for photovoltaic devices, J. Appl. Phys. 114 (2013) 013505.
[40] G.E. Arnaoutakis, J. Marques-Hueso, T.K. Mallick, B.S. Richards, Coupling of sunlight into optical fibres and spectral dependence for solar energy applications, Sol. Energy 93 (2013) 235–243.
[41] G.E. Arnaoutakis, J. Marques-Hueso, A. Ivaturi, K.W. Krämer, T.K. Mallick, B.S. Richards, Enhancement of upconversion for photovoltaics with β-NaYF4: Er3+ and concentrating integrated optics, in: OSA Renewable Energy and the Environment Congress-Optical Nanostructures and Advanced Materials for Photovoltaics, Optical Society of America, Tucson, Arizona, United States, 2013, pp. PT3C. 4.
[42] M. Pollnau, P. Hardman, W. Clarkson, D. Hanna, Upconversion, lifetime quenching, and ground-state bleaching in Nd^{3+}:$LiYF_4$, Opt. Commun. 147 (1998) 203–211.
[43] G. Blasse, B. Grabmaier, Luminescent materials, Springer-Verlag, Berlin/New York, 1994.
[44] F. Auzel, Upconversion and anti-Stokes processes with f and d ions in solids, Chem. Rev. 104 (2004) 139–174.
[45] S. Fischer, A. Ivaturi, B. Fröhlich, M. Rudiger, A. Richter, K.W. Krämer, B.S. Richards, J.C. Goldschmidt, Upconverter silicon solar cell devices for efficient utilization of sub-band-gap photons under concentrated solar radiation, IEEE J. Photovolt. 4 (2014) 183–189.
[46] J. Wang, T. Ming, Z. Jin, J. Wang, L.-D. Sun, C.-H. Yan, Photon energy upconversion through thermal radiation with the power efficiency reaching 16%, Nat. Commun. 5 (2014) 5669.
[47] R. Martín-Rodríguez, S. Fischer, A. Ivaturi, B. Froehlich, K.W. Krämer, J.C. Goldschmidt, B.S. Richards, A. Meijerink, Highly efficient IR to NIR upconversion in Gd_2O_2S:Er^{3+} for photovoltaic applications, Chem. Mater. 25 (2013) 1912–1921.
[48] S. Fischer, J.C. Goldschmidt, E. Favilla, M. Tonelli, Record efficient upconverter solar cell devices with optimized bifacial silicon solar cells and monocrystalline BaY_2F_8:30%Er^{3+} upconverter, Sol. Energy Mater. Sol. Cells 136 (2015) 127–134.
[49] L.C. Hirst, N.J. Ekins-Daukes, Fundamental losses in solar cells, Prog. Photovolt.: Res. Appl. 19 (2011) 286–293.
[50] M.A. Green, Solar cells: operating principles, technology, and system applications, Prentice-Hall, Inc., Englewood Cliffs, NJ, 1982.
[51] J.H. Atwater, P. Spinelli, E. Kosten, J. Parsons, C. Van Lare, J. Van de Groep, J.G. de Abajo, A. Polman, H.A. Atwater, Microphotonic parabolic light directors fabricated by two-photon lithography, Appl. Phys. Lett. 99 (2011) 151113.
[52] J. De Wild, J.K. Rath, A. Meijerink, W.G.J.H.M. Van Sark, R.E.I. Schropp, Enhanced near-infrared response of a-Si: H solar cells with β-$NaYF_4$:Yb^{3+}(18%), Er^{3+}(2%) upconversion phosphors, Sol. Energy Mater. Sol. Cells 94 (2010) 2395–2398.